IChemE

www.ingentaselect.com/titles/02638762.htm

0263–8762/04/$30.00+0.00

Trans IChemE, Part A, February 2004
Chemical Engineering Research and Design, 82(A2): 1–10

COMPARISON OF A MECHANISTIC MODEL FOR NUCLEATE BOILING WITH EXPERIMENTAL SPATIO-TEMPORAL DATA

I. GOLOBIČ[1], E. PAVLOVIČ[1], J. VON HARDENBERG[2], M. BERRY[3], R. A. NELSON[3], D. B. R. KENNING[4] and L. A. SMITH[4,5]

[1]*University of Ljubljana, Ljubljana, Slovenia*
[2]*CIMA, University of Genova, Savona, Italy*
[3]*Los Alamos National Laboratory, Los Alamos, NM, USA*
[4]*Oxford University, Oxford, UK*
[5]*London School of Economics, London, UK*

Mechanistic numerical simulations have been developed for pool nucleate boiling involving large groups of nucleation sites that are non-uniformly distributed spatially and have different activation superheats. The simulations model the temperature field in the heated wall accurately and use approximations for events in the liquid–vapour space. This paper describes the first attempt to compare the numerical simulations with spatio-temporal experimental data at a similar level of detail. The experimental data were obtained during pool boiling of water at atmospheric pressure on a horizontal, electrically heated stainless steel plate 0.13 mm thick. They consist of wall temperature fields measured on the back of the plate by liquid crystal thermography at a sampling rate of 200 Hz over a period of 30 s. Methods of image analysis have been developed to deduce the time, position, nucleation superheat and size of the cooled area for every bubble nucleation event during this period. The paper discusses the methodology of using some of the experimental data as input for the simulations and the remainder for validation. Because of the high-dimensional dynamics and possibly chaotic nature of nucleate boiling, the validation must be based on statistical properties over a large area and a long period. This preliminary study is restricted to a single heat flux.

Keywords:

Q1

INTRODUCTION

Much effort has been devoted to developing mechanistic models for nucleate boiling that include the local variations in wall temperature caused by the non-uniform transfer of heat around nucleation sites. Such models are expected to enhance and eventually replace empirical correlations relating average heat flux to average wall superheat. Numerical simulations of many nucleation sites acting simultaneously are required and this is a considerable challenge. Kunugi *et al.* (2002) performed fully three-dimensional simulations of flow fields containing tens to hundreds of growing bubbles but they assumed random nucleation on a uniformly superheated wall, rather than nucleation at specific sites, and the minimum computational cell size was 0.1 mm, about two orders of magnitude larger than the size required for detailed modelling of evaporation at a triple interface under a growing bubble. At an even less detailed level, numerical models capable of modelling hundreds to thousands of nucleation sites have been developed, for example by Pasamehmetoglu and Nelson (1991) and Golobič *et al.* (1996a, b) for low heat fluxes, and by Sadasivan *et al.* (1995) and He *et al.* (2001) for nucleate boiling at high heat flux in a thin macrolayer. These models calculate conduction within the wall accurately but use macroscopic approximations for events at the solid–fluid interface and in the liquid–vapour space. Consequently, it is highly desirable to validate the models against experimental data at a mechanistic level. Because of the high-dimensional dynamics and possibly chaotic nature of nucleate boiling, validation must be based on statistical properties over a large area and a long period. Nobody yet knows how large and long but this can be tested through invariance of the statistical properties. A further difficulty is that the numerical models require as input the positions and characteristics of the nucleation sites. This information cannot yet be obtained entirely from measurements of surface microgeometry and wetting characteristics. The options are:

(1) to assume a density of sites that are randomly distributed, both spatially and within a specified range of activation superheats;
(2) to measure experimentally the site positions during boiling experiments and to make assumptions about their activation superheats from measurements of the average wall superheat;

*Correspondence to: Dr D. B. R. Kenning, Oxford University, Oxford, UK.
E-mail: david.kenning@eng.ox.ac.uk

(3) to attempt to measure the activation superheats of individual sites during boiling, which may limit the number of sites that can be considered.

Option (1) may be appropriate when using a validated model to predict the behaviour of a group of sites that is sufficiently large for its statistical characteristics to be independent of size. This condition may not be satisfied in many laboratory-scale experiments. Implementing option (2) by optical measurements of bubble sites on the boiling side is feasible only in open geometries at low heat fluxes and does not fully specify the sites. Option (3) is achieved approximately by wall temperature field measurements by liquid crystal or infra-red thermography on the rear surface of an electrically heated, very thin plate. Realistic surface conditions can be used on the boiling side but the limited thermal capacity of the plate and the constraint on lateral conduction modify the physics of boiling. Provided the numerical simulations include these effects, validation for these special conditions would increase confidence in their capability to model other conditions.

This paper is based on liquid crystal data for slightly subcooled water at 96°C and atmospheric pressure boiling on a horizontal stainless steel plate $41 \times 28 \times 0.13$ mm thick. It discusses the methodology of specifying the input data and making comparisons with a numerical simulation code intended for low-flux boiling. The comparisons are here limited to a single value of the uniform input heat flux. (There is no attempt to optimize the model, nor to measure its performance over a range of heat fluxes.) The comparisons are based on 6000 samples of the wall temperature fields from the experimental data and the synthetic data generated by each simulation. Data from the experiment and from a completely successful simulation should have indistinguishable statistical properties. The questions are which data and which statistical properties should be used.

EXPERIMENTAL DATA

The experimental methods and manual analysis of the data are described by Kenning and Yan (1996). The bubble activity on the boiling side of the heated plate and the colourplay of the liquid crystal on the back of the plate were recorded together on each video field at 200 Hz with successive fields interlaced. Hue fields were converted to temperature fields by a calibration. Manual analysis of the simultaneous bubble views and temperature fields showed that each nucleation event caused sudden cooling over the maximum bubble contact area during growth (approximately equal in diameter to the departure diameter) and that this pattern could be used successfully to detect nucleation events without reference to the bubble-side information. By backtracking in time, the local wall superheat immediately preceding nucleation was found and the local instantaneous heat flux into the liquid was calculated from the rate of change of wall temperature. The corresponding temperature gradients in the liquid were found to be sufficiently low, on the scale of the effective site radius, that they should not affect the activation superheat. Manual analysis was too slow to be applied over the long time periods necessary for statistical analysis so a new, fully automated method of image analysis was developed using non-orthogonal empirical functions (NEFs). Each temperature field was reconstructed from bell-shaped NEFs suggested by the bubble cooling pattern. Truncation of the reconstruction combined with an algorithm to recognise the time sequence of temperature changes typical of bubble growth provided an efficient means of identifying nucleation events. The method is described by McSharry *et al.* (2002) and its success in identifying sites when compared with manual identification at low heat flux is described by von Hardenberg *et al.* (2002). The possible misinterpretation of events such as bubble coalescence in a statistical investigation of interactions between nucleation sites is discussed by von Hardenberg *et al.* (2003).

The experimental data used in this paper were derived from a sequence of 6000 temperature fields over 30 s at a heat flux of 50.8 kW m^{-2} for a region 20×11 mm (chosen to exclude edge effects and regions of damaged liquid crystal). They define for each nucleation event its timing, spatial coordinates, activation temperature and the maximum radius of the NEFs describing the local cooling during bubble growth. 2499 events were detected at 1505 locations, with activation superheats in the range 8–23 K and NEF radii in the range 1–5 mm (Figures 1–3). The average site density is about 7 mm^{-2}, but much of the activity occurs in 16 clusters of sites lying within circles with diameters of about 1 mm, comprising 653 out of 1505 sites.

Of the total 2499 events, 1498 occurred in these regions. Many other sites produce only one or two bubbles in 30 s. Uncertainty in the location of sites arises from the resolution of the camera and signal noise affecting the apparent position of the centre of the first NEF in each event. The basic spacing of the array of temperatures is $\Delta_x = 0.1$ mm, $\Delta_y = 0.17$ mm (larger in the y direction because of the interlacing of video fields). Knowing that a 3×3 spatial averaging filter removes most of the signal noise, the uncertainty is estimated to be $\sim 3\Delta_y$, say ± 0.5 mm, to be compared with the average NEF radius of 1.85 mm. Thus it is unclear whether the clusters of activity really are groups of sites interacting strongly with each other, some perhaps depending on vapour seeding from the more stable sites, or whether they are actually single sites at locations that have not been precisely determined. In their preliminary study of site interactions, Kenning and Yan (1996) consolidated the clusters into single sites. Whether to do this for the input data for the numerical models is an issue to be addressed. For sites producing multiple bubbles, the standard deviation

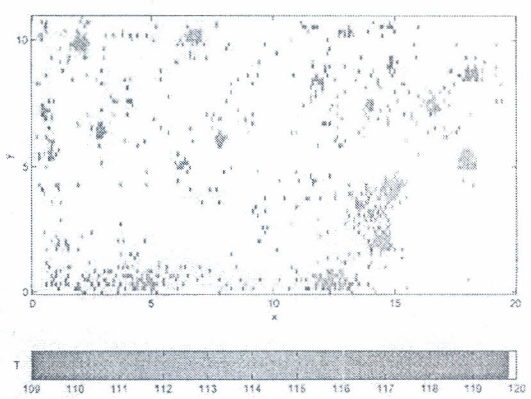

Figure 1. Location and activation temperatures of nucleation events.

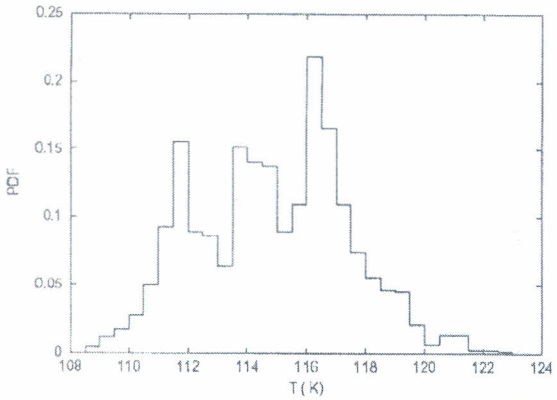

Figure 2. PDF of activation temperatures.

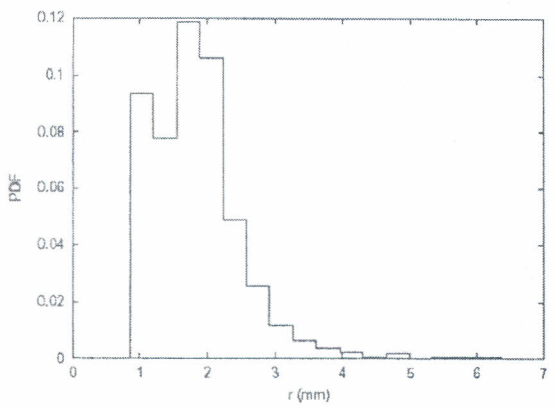

Figure 3. PDF of maximum NEF radii.

of the activation temperature is generally less than 0.5 K. Outside the clusters, the distributed sites with very low levels of activity may be stable sites that are on the threshold of their activation temperature or they may be unstable sites that are very occasionally activated by bubbles from other sites. Again, it is necessary to consider whether to include these sites in the specification of the numerical model. A small variation in the modelling of local wall superheat may switch on or off sites that have a large effect on the spatial distribution of cooling. Some of these issues may be resolved by further analysis, for example at different heat fluxes, that has not yet been performed.

Kenning and Yan (1996) noted that the nature of bubble growth on the same plate was sensitive to the cleaning procedure and consequent contact angle. The data in this paper are for a well-wetted plate with a contact angle ~20°, realized by stringent cleaning with residue-free detergent followed by prolonged rinsing and protection of the surface from contamination up to the instant of immersion. Larger contact angles resulting from less rigorous cleaning led to much smaller bubbles produced at high frequencies beyond the response rate of the liquid crystal. The impression that there were more active sites at large contact angles could not be tested quantitatively. This sensitivity to contact angle must be incorporated in some way in the numerical models.

NUMERICAL SIMULATIONS AND INPUT DATA

Low heat flux models for the discrete-bubble boiling regime have been developed by Golobič *et al.* (1996a, b) and Unal and Pasamehmetoglu (1994). A high heat flux model has been developed by Sadasivan *et al.* (1995). All of these simulations model conduction throughout the thickness of the solid wall accurately. They are capable of modelling the layer of liquid crystal behind the heated stainless steel but the layer has been ignored in this particular exercise. The numerical schemes use irregular meshes that depend on the nucleation site positions, with much greater resolution around each site to resolve the steeper gradients of wall temperature near active sites. The computed temperature fields are interpolated onto a regular grid for comparison with the experimental data.

The simulations require as input the positions of potential sites and activation superheats (effective site sizes) for each of these potential nucleation sites. It is assumed that activation depends only on the local wall superheat. After a period of cooling, bubble nucleation occurs as soon as the wall superheat recovers to the activation value. Temperature gradients in the liquid at the wall are not considered. (They can be shown to be small for the particular conditions of this study.) The effectiveness of sites as vapour traps, seeding–flooding interactions and hydrodynamic interactions between sites (Zhang and Shoji, 2003) are not considered.

The major difference in the various mechanistic models is their approximate representation of the fluid side of the problem. This paper employs the discrete-bubble, low-heat-flux model of Golobič *et al.* (1996a, b) to provide simulated data for the spatio-temporal boiling processes for comparison with the experimental data. The purpose is to explore how to go about such a comparison, not to determine whether the model of Golobič *et al.* is good or bad. So far as the authors are aware, a comparison of this sort based on spatio-temporal behaviour has not been undertaken previously.

The model is summarized in the Appendix. Growing bubbles are modelled as truncated spheres defined by an apparent contact angle. In the experiments, examination of a small number of the larger bubbles showed that cooling of the wall occurred over an apparent contact region with radius only slightly smaller than the bubble radius, even though the wall was well-wetted (Kenning and Yan, 1996). It may therefore be necessary to use an artificially high value of apparent contact angle to reconcile the distortion of bubbles near the wall with the modelling assumption of a truncated sphere. This apparent contact angle must be distinguished from the real contact angle that has the marked effect on the mode of bubble growth noted above. Growth stops at a departure radius that may be defined by a correlation but which is here taken to correspond to a base radius equal to the measured average value of the radius of the NEF corresponding to maximum cooling during all the growth events at a particular site. Consequently, there are no variations in size between simulated bubbles at a particular site, only between bubbles from different sites. The entire heat input driving bubble growth is assumed to be drawn from the wall by evaporation at a triple interface of microscopic width and high heat transfer coefficient, for which values are estimated. The inner contact region is assumed to be covered by an adsorbed film and some residual liquid trapped in the surface roughness. In this particular version of

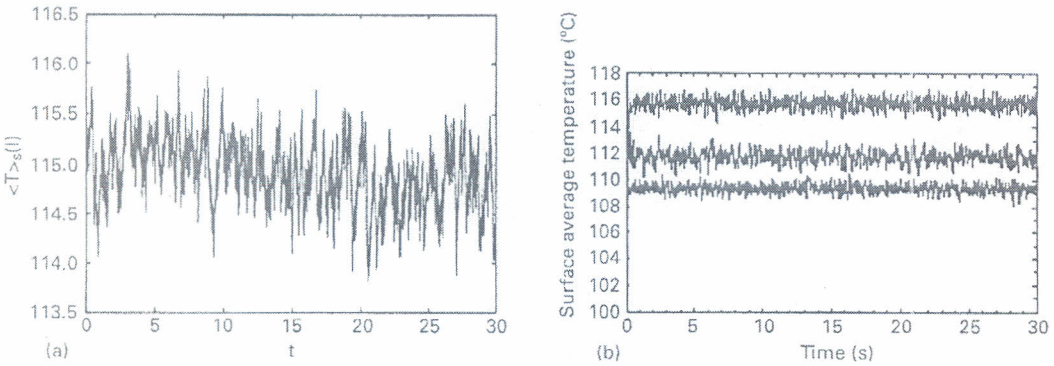

Figure 4. Temporal variation of spatial average wall temperature (a) experimental, (b) simulated for 1505 sites (lowest), 414 sites (middle) and 66 sites (top).

the model, heat input to the spherical part of the bubble from the superheated boundary layer is neglected.

Any wall area not directly under a growing bubble is subjected to a conventional natural convection heat transfer coefficient. Limited examination of the experimental data suggested that there was a general enhancement of the single phase heat transfer coefficient during the recovery period between bubbles, Kenning and Yan (1996). Enhancement has not been assumed in these simulations.

The assumed absence of long-range interactions between nucleation sites is supported by the analysis of the experimental data by von Hardenberg *et al.* (2003). However, other experiments on interactions between controlled pairs of nucleation sites (Gjerkeš and Golobič, 2002; Zhang and Shoji, 2003), do indicate influences extending beyond the bubble contact areas. The 20×11 mm region from which the experimental data are taken may be influenced by unspecified sites lying just outside the region. The simulation is therefore extended 1.85 mm beyond each edge, although the data are analysed only in the region coinciding with the experimental data. In this case, it is assumed that the outer border does not contain any nucleation sites. An alternative would be to distribute sites randomly, at the same density as the inner region.

It is evident that mechanistic modelling at this level involves significant approximations that can be improved. Validation tests should suggest where improvements are required.

VALIDATION

The experiment and the simulations are spatio-temporal systems that can have complex dynamics. Assuming that, at constant heat flux, they reach equilibrium, their statistical properties become constant if measured over a sufficiently long time. The experimental data defines the positions, activation superheats and average bubble base radii for potential sites in the simulations. The problem of sites with low activity was attacked here by performing three simulations, firstly with all the 1505 experimental sites, then with the 414 sites that produced at least two bubbles in 30 s and finally with the 66 sites that produced at least five bubbles in 30 s. The temporal behaviour of the spatially averaged temperature for experiment and simulations are shown in Figure 4 to provide an indication of how the number of active sites affects the simulations.

Table 1 provides a comparison of the simulations with experiment based on global parameters. In all cases, the number of sites active in the simulation is less than the number of potential sites, indicating that the simulation had sufficient sites for flexible dynamic behaviour and suggesting strong thermal interactions between the sites. Despite this, the number of bubbles produced in the simulations is significantly higher than the number in the experiment. The simulation with the smallest number of sites is closest to the experiment. It overestimates the space–time averaged wall superheat by less than 6%. However, it overestimates the production of bubbles by 50%, so its mechanistic performance is poor. In the remainder of this section, other statistical properties are compared for the experimental data and the simulations, with consideration given primarily to the cases with 1505 and 66 potential sites.

The spatial distributions of time-averaged temperature are shown in Figure 5. They depend on the distribution of the active sites and also on their activation superheats. All the simulations overestimate the amplitude of the variations in time-averaged temperature. The values of the average spatial variance $\langle \sigma^2 \rangle$ (computed for all fields and then averaged) are 3.75 and 21.7 for the experimental data and the simulation with 66 sites, respectively. This is consistent with the overestimation of bubble production and the associated latent heat flux. From visual inspection of Figure 5, it appears that the simulation with the smallest number of active sites (d) best

Table 1. Global comparison of simulations and experiment.

		Number of bubbles in 30 s		Average ΔT (K)	
Number of potential sites	Number of active sites	Simulation	Experiment	Simulation	Experiment
(1+) 1505	352	14063	2499	9.4	14.9
(2+) 414	155	5901	2499	11.8	14.9
(5+) 66	32	3742	2499	15.7	14.9

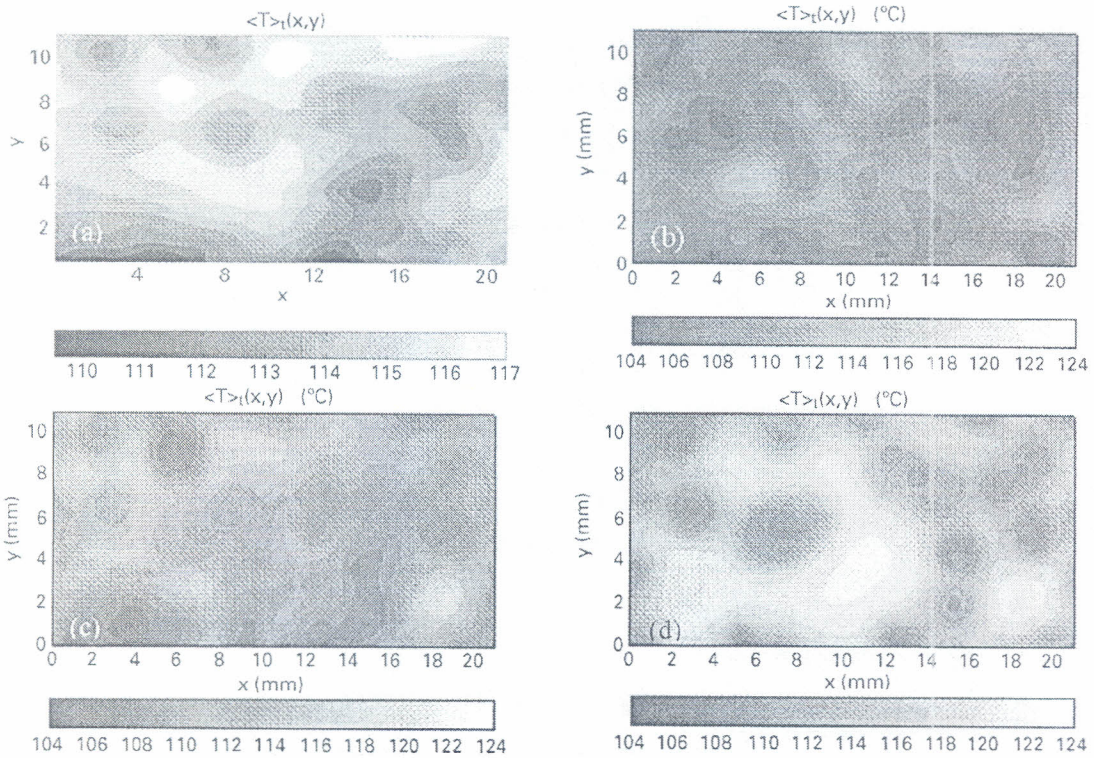

Figure 5. Isotherms of spatio-temporal average wall temperatures: (a) experimental, (b) simulation 1505 sites, (c) simulation 414 sites, (d) simulation 66 sites.

captures the spatial characteristics of the experimental data. Further statistical analysis shows that there is actually little difference between the simulations with 1505 and 66 sites in this respect.

The one-dimensional power spectra of the spatial variations in the x and y directions are shown in Figure 6. They were obtained, for example in the x direction, by computing the spectra for every row in every field and then averaging for all rows and all times. For a sufficiently large system, the spectra would be expected to be independent of direction but in this case there are some differences at the smaller length scales. For a given direction, the spectra for the two simulations are almost the same for wavelengths λ from 5 down to 0.7 mm. The similarities between the simulations may be a consequence of additional sites contributing to the clustering effect but, as would be expected, the simulation with fewer sites has more power in the variations at large length scales. The spectra for the simulations lie well above the spectrum for the experimental data, also as expected from the relative values of variance, but they have similar gradients for length scales above 2 mm (i.e. above the mean bubble radius). The differences at smaller length scales may be due to the details of simulating bubble growth, or possibly the effects of bubble coalescence.

To provide insight into the time-dependent aspects of the comparison, the power spectra for temporal variations, obtained by averaging the individual temporal power spectra at all grid points, are shown in Figure 7. The spectra for the simulations are in close agreement with each other for time intervals below 300 ms. Above 300 ms, there is a sharp and

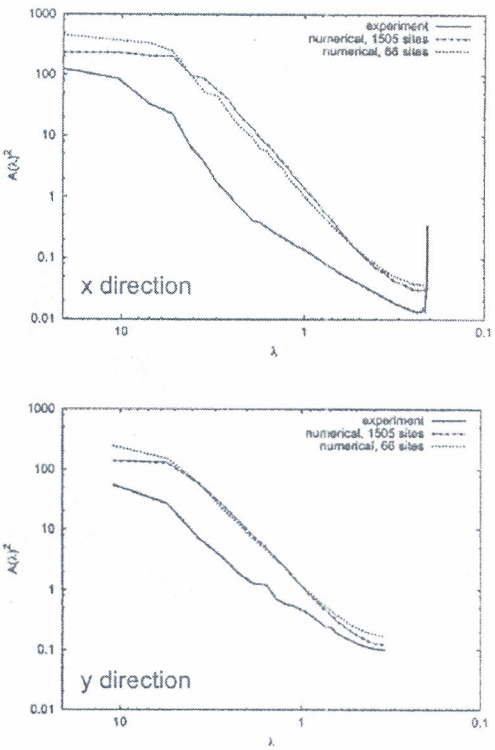

Figure 6. Power spectra of temperature with respect to wavelength λ (mm).

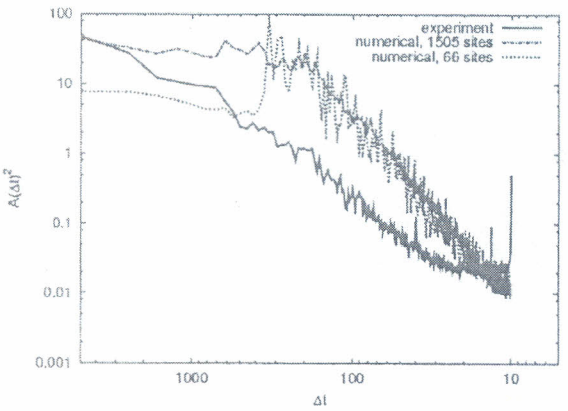

Figure 7. Power spectra in time (ms) averaged over all grid points.

for now unexplained, fall in the power spectrum for the simulation with the small number of sites. The simulated spectra are completely different in character from the experimental spectrum. Between 300 and 20 ms, the typical experimental bubble growth time, the simulated spectra lie above the experimental spectrum. This is consistent with the previous indications that the simulations overestimate the bubble production rate and the amplitude and frequency of the variations in the wall temperature field. Below 20 ms, the spectra cross over, suggesting that the simulations underestimate the amplitude of the temperature depressions under growing bubbles. This is also consistent with the overestimate of bubble frequency, implying that less heat is removed from the wall per bubble. For the conditions of these particular experiments, the bubble frequency depends mainly on the recovery time between bubbles, which in turn depends on the initial depression in temperature and on the single phase heat transfer coefficient during recovery, rather than the bubble growth time. Use of an enhanced single phase heat transfer coefficient and optimisation of the combination of apparent contact angle and triple contact line heat transfer coefficient should therefore be investigated as ways of improving the simulation. Further information should be obtainable by statistical analysis of the heat extracted from the wall, which can be estimated directly from the NEF analysis.

Other statistical properties related to bubble production, such as distributions of bubble size and activation temperature, are of limited value for validation because the experimental distributions are input data for the simulations. Any deviations arise because of the way the simulations select active sites from the potential (i.e. experimental) sites.

CONCLUDING DISCUSSION

This first attempt at validating a semi-mechanistic simulation has highlighted several areas of difficulty:

(1) The specification of the population of potentially active sites starts from the experimental observation of actual sites, many of which are of very low activity. Analysis of data at increasing heat fluxes may show whether this is due to sites being on the threshold of their activation temperature. Further analysis of data at a single heat flux may show whether these sites are unstable and depend on seeding by adjacent sites. This possibility is not at present included in the simulation.

(2) The simulated bubble frequency is too high. This may be due to a general increase in the single-phase heat transfer rate, caused by rising bubbles and by non-uniform circulation in the boiling vessel, and under-prediction of the cooling under individual bubbles.

(3) The over-prediction of bubble production at clusters of sites leads to spatial variations in temperature that are too high. Further analysis is required of the latent heat flux in the simulations, calculated from the production rates of bubbles of a size specified from the experimental data and calculated from the experimental transient changes in wall temperature.

(4) It is clearly desirable to increase the area of observation to include many more fully-active sites and to reduce edge effects. This is well within the capabilities of the simulations but may be limited experimentally by the spatial resolution of video cameras. The characteristics of liquid crystal thermography impose a severe limit on the temporal resolution, which may be avoidable by using high-speed infra-red thermography.

The statistical comparisons have indicated some relatively straightforward ways of improving the simulation. There are a number of other features of the simulation that require further development. In particular, the departure sizes of bubbles should be modelled, rather than specified from the experimental data. The present criterion for activity of a site is very simple and only thermal interactions between sites by conduction in the wall are considered. Bubble coalescence is not at present included in the simulation. Statistical analysis of the experimental data by von Hardenberg *et al.* (2003) to detect interactions indicated that bubble coalescence should be examined more closely and Zhang and Shoji (2003) identified coalescence as an important mechanism for increasing site activity.

APPENDIX: SUMMARY OF NUMERICAL SIMULATION

Computational Model

Energy equation:

$$\frac{\partial T}{\partial \tau} = \frac{\lambda_H}{\rho_H c_{pH}}\left[\frac{\partial^2 T}{\partial x^2} + \frac{\partial^2 T}{\partial y^2} + \frac{\partial^2 T}{\partial z^2}\right] + \frac{\dot{q}}{\rho_H c_{pH} \delta_H} \qquad \text{(A1)}$$

Boundary of computational area at saturation temperature

$$T|_{x=0,x=x_{ca},y=0,y=y_{ca},0\le z\le \delta_H} = T_{sat} \qquad \text{(A2)}$$

At the bottom surface, heat transfer to surrounding air

$$\left.\frac{\partial T}{\partial z}\right|_{0\le x\le x_{ca},0\le y\le y_{ca},z=0} = \alpha_{air}(T - T_{air}) \qquad \text{(A3)}$$

At the upper surface, heat transfers to fluid in two areas, as in Figure A1: active nucleation site areas, and natural convection area.

Growing bubbles are modelled to be radially symmetrical truncated spheres, defined by contact angle ϕ. Bubble

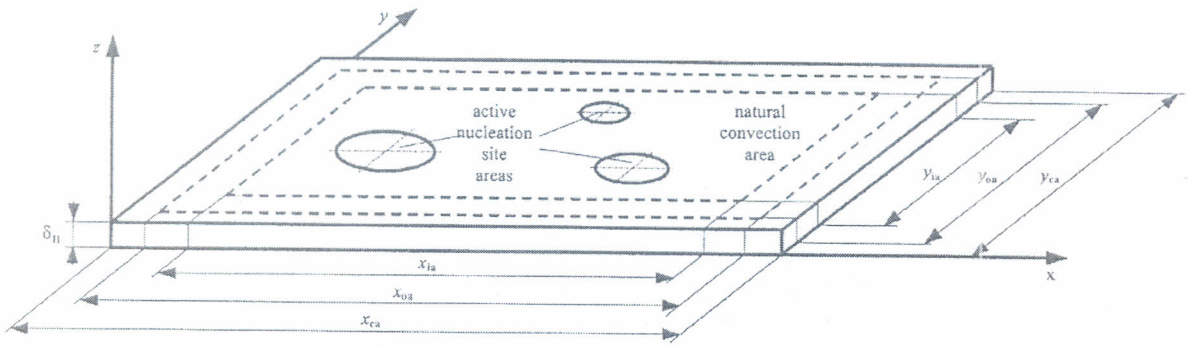

Figure A1. Computational model.

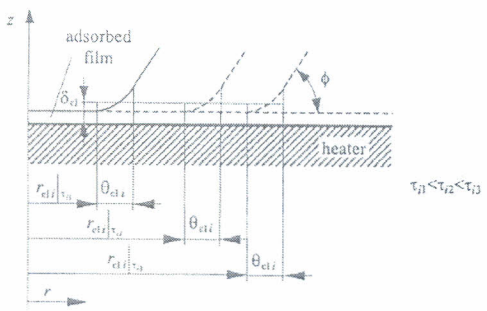

Figure A2. Bubble growth in nucleation site *i*.

growth in nucleation site *i* area is schematically shown in Figure A2.

In contact line area of width θ_{cli} between adsorbed film and the rest of the liquid the thickness of the liquid wedge is represented by an averaged and constant value δ_{cl}. Heat transfer coefficient for nucleation site *i* due to evaporation of liquid in the contact line area during bubble growth τ_i is

$$\alpha_{cl}|_{r_{cli}|_{\tau_i}\le r\le r_{cli}|_{\tau_i}+\theta_{cli},z=\delta_H}=\frac{\lambda_L}{\delta_{cl}} \tag{A4}$$

Because the roughness of the heating surface may retain liquid under the growing bubble, the heat transfer coefficient α_f due to heat transfer over the adsorbed film and evaporation of

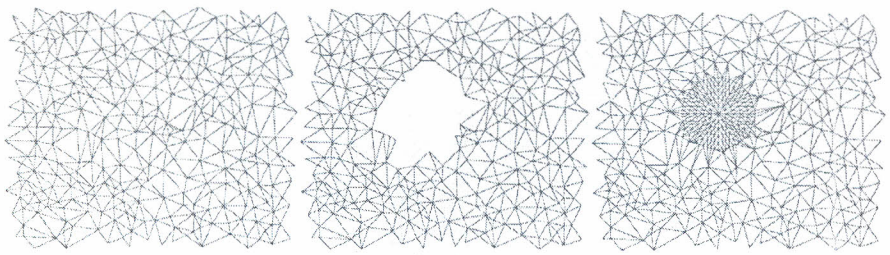

Figure A3. Mesh modification following activation of a nucleation site.

Table A1. Nucleation site procedure from activation to deactivation.

Activation of nucleation site *i*	$(T\|_{x=x_{nsi},y=y_{nsi},z=\delta_H} > T_{acti}) \wedge \left(\sqrt{(x_{nsi}-x_{nsj})^2+(y_{nsi}-y_{nsj})^2} \le 1.12(r_{bdi}+r_{bdj})\sin\phi\right) \Rightarrow \tau_i = 0$ $j \in \{\text{surrounding nucleation sites}\}$
	$r_{bi}\|_{\tau_i=0} = 0$
	$Q_{bi}\|_{\tau_i=0} = 0$
	$r_{cli}\|_{\tau_i=0} = 0$
Bubble growth in nucleation site *i* for each time step $\Delta\tau$	$Q_{bi}\|_{\tau_i+\Delta\tau} = Q_{bi}\|_{\tau_i} + \left[\pi r_{cli}^2\|_{\tau_i}\alpha_{fi}\|_{0\le r<r_{cli}\|_{\tau_i},z=\delta_H}\left(T\|_{0\le\sqrt{(x-x_{nsi})^2+(y-y_{nsi})^2}<r_{cli}\|_{\tau_i},z=\delta_H} - T_{sat}\right)\right.$ $\left. +2\pi r_{cli}\|_{\tau_i}\theta_{cli}\alpha_{cl}\|_{r_{cli}\|_{\tau_i}\le r\le r_{cli}\|_{\tau_i}+\theta_{cli},z=\delta_H}\left(T\|_{r_{cli}\|_{\tau_i}\le\sqrt{(x-x_{nsi})^2+(y-y_{nsi})^2}\le r_{cli}\|_{\tau_i}+\theta_{cli},z=\delta_H} - T_{sat}\right)\right]\Delta\tau$
	$r_{bi}\|_{\tau_i+\Delta\tau} = \sqrt[3]{\dfrac{Q_{bi}\|_{\tau_i+\Delta\tau}}{\rho_V\Delta h_{fg}(\pi[2-\cos\phi][1+\cos\phi]^2/3)}}$
	$r_{cli}\|_{\tau_i+\Delta\tau} = r_{bi}\|_{\tau_i+\Delta\tau}\sin\phi$
Deactivation of nucleation site *i*	$r_{bi}\|_{\tau_i+\Delta\tau} \ge r_{bdi}$

Table A2. Parameters of computation.

Heater side					Inner area		Outer area		Comparison area	
	ρ_H (kg m^{-3})	c_{pH} (J kg^{-1} K^{-1})	λ_H W (m K)$^{-1}$	δ_H μm	x_{ia} (mm)	y_{ia} (mm)	x_{oa} (mm)	y_{oa} (mm)	x_{ca} (mm)	y_{ca} (mm)
	7900	520	16.3	125	21	11	24.5	14.5	27.322	16.87
Bottom side			T_{air} (°C) 100					α_{air} (W m^{-2} K^{-1}) 5		
Top side	T_{sat} (°C)	Δh_{fg} (kJ kg^{-1})	ρ_V (kg m^{-3})	ρ_L (kg m^{-3})	c_{pL} (J (kg K)$^{-1}$)	λ_L (W m^{-1} K^{-1})	ν_L (m^2 s^{-1})	γ (°C^{-1})	α_{ns} (W m^{-2} K^{-1})	
	100	2257	0.597	958.1	4216	0.677	2.94×10^{-8}	2.879×10^{-3}	equation (A9)	
Computational parameters		Q (kW m^{-2}) 50.8			τ (s) 30			$\Delta\tau$ (μs) 40		
Nucleation site parameters	ϕ (deg) 32			δ_{cl} (mm) 500		α_{cl} (W m^{-2} K^{-1}) λ_L/δ_{cl}		θ_{clf} (μm) $r_{bdf} \sin\phi/M_r$	α_{tf} (W m^{-2} K^{-1}) $30{,}000 - 25{,}000r/r_{clf}(\tau_t)$	
		N_{ns}	x_{nsi} (mm)		y_{nsi} (mm)			T_{acti} (°C)	r_{bdf} (mm)	
	Inner area	1505	$x_{nsi} \in \left\{\frac{x_{ca}-x_{ia}}{2}, x_{ca}-\frac{x_{ca}-x_{ia}}{2}\right\}$		$y_{nsi} \in \left\{\frac{y_{ca}-y_{ia}}{2}, y_{ca}-\frac{y_{ca}-y_{ia}}{2}\right\}$			108.39	1.03	
			position from NEF analysis data					122.35	6.19	
	Outer area (to reduce edge effect)	95	$x_{nsi} \in \left\{\frac{x_{ca}-x_{oa}}{2}, \frac{x_{ca}-x_{ia}}{2}\right\} \vee \left\{x_{ca}-\frac{x_{ca}-x_{ia}}{2}, x_{ca}-\frac{x_{ca}-x_{oa}}{2}\right\}$		$y_{nsi} \in \left\{\frac{y_{ca}-y_{oa}}{2}, \frac{y_{ca}-y_{ia}}{2}\right\} \vee \left\{y_{ca}-\frac{y_{ca}-y_{ia}}{2}, y_{ca}-\frac{y_{ca}-y_{oa}}{2}\right\}$			115.5	2	
			random position							
	Comparison area (to reduce edge effect)	0	—		—			—	—	
			$T\|_{\tau=0, x=x_{ca}, x=0, y=y_{ca}, 0 \le z \le \delta_{cl}} = T_{sat}$							
Numerical parameters		M_{bas}		M_{ns}			M_r		M_z	
		13,950		181			5		5	

the remaining liquid is obtained from comparison of temperature field measurements with computed temperature fields

$$\alpha_{\mathrm{f}i}|_{0\le r<r_{\mathrm{cl}i}|_{\tau_i},z=\delta_{\mathrm{H}}} = f\left[\left.\frac{r}{r_{\mathrm{cl}i}}\right|_{\tau_i}\right] \tag{A5}$$

The transferred heat for bubble growth at a nucleation site i at new time $\tau+\Delta\tau$ is

$$\begin{aligned} Q_{\mathrm{b}i}|_{\tau_i+\Delta\tau} &= Q_{\mathrm{b}i}|_{\tau_i} + \left[\pi r_{\mathrm{cl}i}^2|_{\tau_i}\alpha_{\mathrm{f}i}|_{0\le r<r_{\mathrm{cl}i}|_{\tau_i},z=\delta_{\mathrm{H}}}\right. \\ &\times\left(T|_{0\le\sqrt{(x-x_{\mathrm{ns}i})^2+(y-y_{\mathrm{ns}i})^2}<r_{\mathrm{cl}i}|_{\tau_i},z=\delta_{\mathrm{H}}} - T_{\mathrm{sat}}\right) \\ &+ 2\pi r_{\mathrm{cl}i}|_{\tau_i}\theta_{\mathrm{cl}i}\alpha_{\mathrm{cl}i}|_{r_{\mathrm{cl}i}|_{\tau_i}\le r\le r_{\mathrm{cl}i}|_{\tau_i}+\theta_{\mathrm{cl}i},z=\delta_{\mathrm{H}}} \\ &\times\left(T|_{r_{\mathrm{cl}i}|_{\tau_i}\le\sqrt{(x-x_{\mathrm{ns}i})^2+(y-y_{\mathrm{ns}i})^2}\le r_{\mathrm{cl}i}|_{\tau_i}+\theta_{\mathrm{cl}i},z=\delta_{\mathrm{H}}}\right. \\ &\left.\left.- T_{\mathrm{sat}}\right)\right]\Delta\tau \end{aligned} \tag{A6}$$

Bubble radius at new time is calculated from

$$r_{\mathrm{b}i}|_{\tau_i+\Delta\tau} = \sqrt[3]{\frac{Q_{\mathrm{b}i}|_{\tau_i+\Delta\tau}}{\rho_{\mathrm{V}}\Delta h_{\mathrm{fg}}(\pi[2-\cos\phi][1+\cos\phi]^2/3)}} \tag{A7}$$

Radial location of contact line is

$$r_{\mathrm{cl}i}|_{\tau_i+\Delta\tau} = r_{\mathrm{b}i}|_{\tau_i+\Delta\tau}\sin\phi \tag{A8}$$

Q2 Heat transfer coefficient in natural convection area (Han and Griffith, 1965)

$$\alpha_{\mathrm{nc}} = 0.14\rho_{\mathrm{L}}c_{\mathrm{pL}}\left[\frac{\gamma g(T-T_{\mathrm{sat}})(\lambda_{\mathrm{L}}/\rho_{\mathrm{L}}c_{\mathrm{pL}})^2}{\nu_{\mathrm{L}}}\right]^{1/3} \tag{A9}$$

Initial Conditions

Temperature of heater at $\tau=0$ is

$$T|_{0\le x\le x_{\mathrm{ca}},0\le y\le y_{\mathrm{ca}},0\le z\le\delta_{\mathrm{H}}} = T_{\mathrm{sat}} + 10^{\circ}\mathrm{C} \tag{A10}$$

Input Parameters

Input parameters for the model are:

- heater side (conductivity, density, specific heat, thickness, dimension of inner, outer and computational area);
- fluid side (saturation temperature, evaporation heat, vapour density, liquid density, liquid specific heat, liquid conductivity, liquid kinematic viscosity, contact angle, thickness of adsorbed film, width of contact line);
- heat flux;
- nucleation site parameters (number of nucleation sites, position of nucleation site (in x-y plane), activation temperature, bubble departure radius).

Solving Computational Model

The main task of the computational model is to calculate temperature fields in the inner area. In the area not covered by growing bubbles there is natural convection given by equation (A9). A bubble starts to grow from nucleation site i when activation temperature $T_{\mathrm{act}i}$ of nucleation site is achieved and that there is no other active nucleation sites in vicinity. The time of bubble growth τ_i is set to zero. The algorithm for mesh modification following activation is based on the Chimera grid technique. To ensure easier generation of the computational mesh the smallest distance between two active nucleation sites i and j was set to 1.12 $(r_{\mathrm{bd}i}+r_{\mathrm{bd}j})\sin\phi$. Computational points that are in an area of $\pi(r_{\mathrm{bd}i}\sin\phi)^2$ are excised from the basic numerical mesh and a radial mesh is inserted. Connections between the basic and radial meshes are performed by Voronoi tesselation. An example of computational mesh modification during activation of a nucleation site is shown in Figure A3. A nucleation site remains active until growth of a bubble stops at a defined bubble departure radius $r_{\mathrm{bd}i}$. Then the nucleation site becomes inactive and heat removal by natural convection is resumed. Mesh modification is performed in reverse order to the description above. The criteria for activation of nucleation sites, bubble growth and deactivation of sites are shown in Table A1.

The energy equation (A1) is solved explicitly by a finite volume method. The computational parameters are shown in Table A2.

NOMENCLATURE FOR APPENDIX

c_{p}	specific heat, J (kg K)$^{-1}$
g	gravity, m s^{-2}
i,j	index
M_{bas}	number of computational points in basic numerical mesh
M_{ns}	number of computational points in a nucleation site numerical mesh
M_r	number of computational points in a nucleation site in radial direction
M_z	number of computational points in z-axis
N_{ns}	number of nucleation sites
q	heat flux, W m^{-2}
Q	heat transfer rate, W
$\dot{q}$	rate of energy generation per unit volume, W m^{-3}
r	radius, m
r_{b}	bubble radius, m
r_{bd}	bubble departure radius, m
r_{cl}	radius of contact line, m
T	temperature, °C
x, y, z	coordinates, m

Greek symbols

α	heat transfer coefficient, W m^{-2} K^{-1}
Δh_{fg}	evaporation heat, J kg^{-1}
$\Delta\tau$	time step, s
δ	thickness, m
ϕ	apparent contact angle, deg
γ	volumetric thermal expansion coefficient, K^{-1}
λ	thermal conductivity, W m^{-1} K^{-1}
ν	kinematic viscosity, m^2 s^{-1}
ρ	density, kg m^{-3}
τ	time, s

Indices

act	activation
ca	computational area
f	adsorbed film
H	heater

ia	inner area
L	liquid
nc	natural convection
ns	nucleation site
oa	outer area
sat	saturation
V	vapour

REFERENCES

Gjerkeš, H. and Golobič, I., 2002, Measurement of certain parameters influencing activity of nucleation sites in pool boiling, *Exp Therm Fluid Sci*, 25: 487–493.

Golobič, I., Pavlovič, E., Strgar, S., Kenning, D.B.R. and Yan, Y., 1996a, Wall temperature variations during bubble growth on a thin plate: computations and experiments, in *Proceedings Eurotherm Seminar, No. 48, Pool Boiling*, Paderborn, 18–20 September 1996, pp 25–32.

Golobič, I., Pavlović, E. and Strgar, S., 1996b, Computer model for nucleation site interactions on a thin plate, in *Proceedings Eurotherm Seminar, No. 48, Pool Boiling*, Paderborn, 18–20 September 1996, pp 33–42.

He, Y., Shoji, M. and Maruyama, S., 2001, Numerical study of high heat flux pool boiling heat transfer, *Int J Heat Mass Transfer*, 44: 2357–2373.

Kenning, D.B.R. and Yan, Y., 1996, Pool boiling heat transfer on a thin plate: features revealed by liquid crystal thermography, *Int J Heat Mass Transfer*, 39: 3117–3137.

Kunugi, T., Saito, N., Fujita, Y. and Serizawa, A., 2002, Direct numerical simulation of pool and forced convection flow boiling phenomena, in *Proceedings of 12th International Heat Transfer Conference*, Grenoble, 18–23 August 2002, Vol 3, pp 497–502.

McSharry, P.E., Ellepola, J.H., von Hardenberg, J., Smith, L.A., Kenning, D.B.R. and Judd, K., 2002, Spatio-temporal analysis of nucleate pool boiling: identification of nucleation sites using non-orthogonal empirical functions, *Int J Heat Mass Transfer*, 45: 237–253.

Pasamehmetoglu, K.O. and Nelson, R.A., 1991, Cavity-to-cavity interaction in nucleate boiling: the effect of conduction within the heater, *AIChE Symp Ser*, 283(87): 342–351.

Sadasivan, P., Unal, C. and Nelson, R.A., 1995, Nonlinear aspects of high heat flux nucleate boiling heat transfer, *J Heat Transfer*, 117: 981–989.

Unal, C. and Pasamehmetoglu, K.O., 1994, Spatial and temporal variations of surface temperature and heat flux for the saturated pool nucleate boiling at lower heat fluxes, *ASME HTD Fund Phase Change Boil Condens*, 273: 49–56.

von Hardenberg, J., Kono, T., Kenning, D.B.R., McSharry, P.E. and Smith, L.A., 2002, Identification of boiling nucleation sites by non-orthogonal empirical functions (NEF) analysis of thermographic data, in *Proceedings of 12th International Heat Transfer Conference*, Grenoble, 18–23 August 2002, 3: 377–382.

von Hardenberg, J., Kenning, D.B.R. and Xing, H., 2003, Nucleation site interactions, in *5th International Conference on Boiling*, Montego Bay, 5–8 May 2003.

Zhang, L. and Shoji, M., 2003, Nucleation site interaction in pool boiling on the artificial surface, *Int J Heat Mass Transfer*, 46: 513–522.

ACKNOWLEDGEMENT

Portions of this research were supported by EPSRC grant GR/M 89034.

The manuscript was received 26 August 2003 and accepted for publication 11 November 2003.